ATLAS Self-Siphoning Rain Gauge Error Estimates*

YOLANDE L. SERRA AND PATRICK A'HEARN

Joint Institute for the Study of Atmosphere and Ocean, Seattle, Washington

H. PAUL FREITAG AND MICHAEL J. MCPHADEN

NOAA/Pacific Marine Environmental Laboratory, Seattle, Washington

(Manuscript received 25 January 2001, in final form 25 May 2001)

ABSTRACT

This report describes sampling and error characteristics of self-siphoning rain gauges used on moored buoys designed and assembled at NOAA's Pacific Marine Environmental Laboratory (PMEL) for deployment in the tropical Pacific and Atlantic Oceans in support of climate studies. Self-siphoning rain gauges were chosen for use on these buoys because they can be calibrated at PMEL before and after deployment. The rainfall data are recorded at 1-min intervals, from which daily mean rate, standard deviation, and percent time raining are calculated and telemetered to PMEL in real time. At the end of the deployment, the 1-min, internally recorded data are recovered and processed to produce 10-min rain rates.

Field data from a subset of these rain gauges are analyzed to determine data quality and noise levels. In addition, laboratory experiments are performed to assess gauge performance. The field data indicate that the noise level during periods of no rain is 0.3 mm h^{-1} for 1-min data, and 0.1 mm h^{-1} for 10-min data. The estimated error in the derived rain rates, based on the laboratory data, is 1.3 mm h^{-1} for 1-min data, and 0.4 mm h^{-1} for 10-min data. The error in the real-time daily rain rates is estimated to be at most 0.03 mm h^{-1}. These error estimates do not take into account underestimates in accumulations due to effects of wind speed on catchment efficiency, which, though substantial, may be correctable. Estimated errors due to evaporation and sea spray, on the other hand, are found to be insignificant.

1. Introduction

Accurate, widespread measurements of precipitation remain critical for several aspects of climate related studies. Freshwater fluxes are an indirect measure of local latent heating, which drives atmospheric circulations. These buoyancy-driven circulations are especially important in the Tropics, where they compose the upward branches of the Hadley and Walker cells. Freshwater fluxes are also important to upper ocean processes, affecting ocean mixed layer temperature and stratification.

Currently, we rely on a combination of satellite and in situ measurements, often in the form of blended products (Huffman et al. 1995; Xie and Arkin 1997; Janowiak and Xie 1999), as a measure of global precipitation. Satellite data, while providing good spatial coverage, are an indirect measure of precipitation and therefore require complicated algorithms to convert to rainfall amount. While in situ rain gauges are potentially more accurate, over the open ocean they are confined to atolls and small islands, which are not distributed in such a way as to sample all the important oceanic rainfall regimes. Moreover, island effects may contaminate these records.

In this study we describe a method for collecting long moored time series in situ rainfall measurements made from Autonomous Temperature Line Acquisition System (ATLAS) buoys located throughout the tropical Pacific and Atlantic Oceans. These buoys, which compose most of the Tropical Atmosphere–Ocean/Triangle Trans-Ocean Buoy Network (TAO/TRITON) array and the entire Pilot Research Moored Array in the Tropical Atlantic (PIRATA) array, are equipped with R. M. Young Company self-siphoning rain gauges. Early attempts to collect rainfall on TAO buoys made use of mini optical rain gauges (ORGs), which were deployed in the west Pacific warm pool region as part of the extended observation period for the Tropical Ocean Global Atmosphere Coupled Ocean–Atmosphere Response Experiment (TOGA COARE) (Godfrey et al. 1998; Cronin and McPhaden 1998). However, the mini optical rain

* Joint Institute for the Study of Atmosphere and Ocean Contribution Number 809 and NOAA/Pacific Marine Environmental Laboratory Contribution Number 2302.

Corresponding author address: Dr. Yolande Serra, NOAA/PMEL, 7600 Sand Point Way NE, Seattle, WA 98115.
E-mail: serra@pmel.noaa.gov

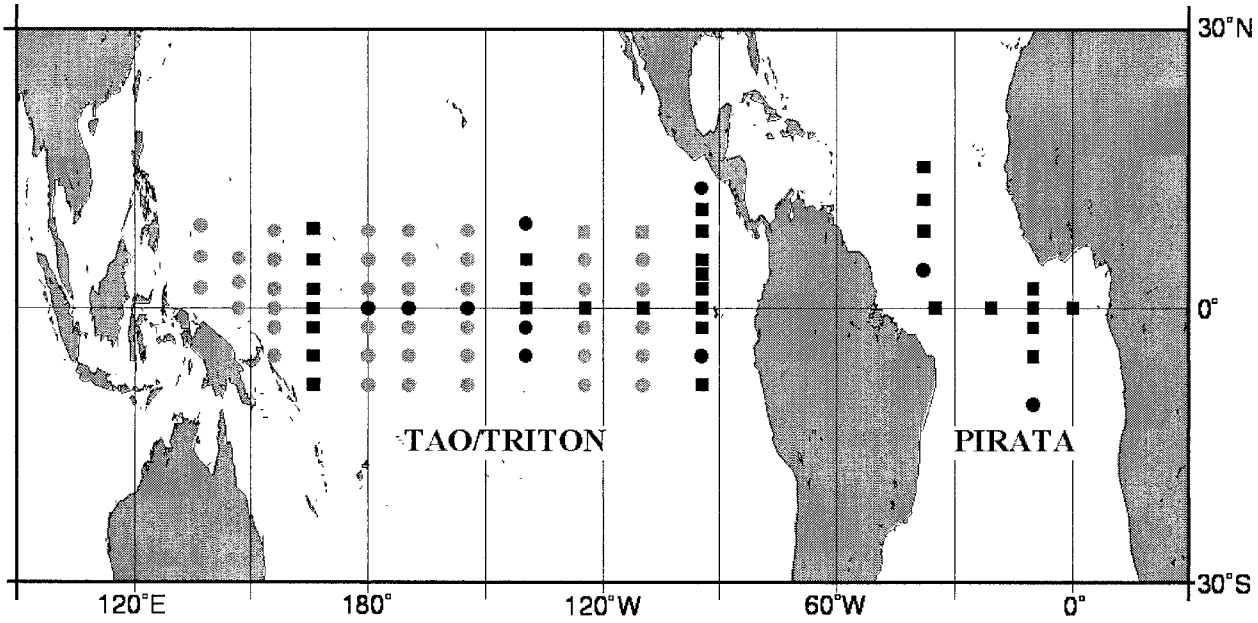

FIG. 1. Map of TAO/TRITON and PIRATA moored buoy arrays. TRITON buoys are located west of 165°E (i.e., along the three westernmost lines). The remaining buoys in the Pacific, and all buoys in the Atlantic, are ATLAS buoys. Also shown are the PACS ATLAS buoys in the east Pacific along 95°W at 3.5°, 10°, and 12°N. Squares indicate the buoys used for this study. Dark circles and squares indicate buoys currently equipped with R.M. Young self-siphoning rain gauges. The two buoys at 8°N, 125°W and 8°N, 110°W (lighter squares) no longer have rain gauges.

gauges were found to be not well suited for buoy applications due to difficulties calibrating them in natural rain. Analysis of duplicate ORGs on the same mooring indicates errors on the order of 15%–25% (Thiele et al. 1995). Instrumentation for rain measurements on ATLAS buoys transitioned from mini ORGs to self-siphoning rain gauges between 1995 and 1998. The R. M. Young rain gauge can be calibrated before and after deployment, improving the reliability of the measurements. Self-siphoning rain gauges also require less power, making them better suited for long-term deployments than ORGs.

The TAO/TRITON array consists of approximately 70 ATLAS and TRITON buoys between 8°S and 8°N, and 137°E and 95°W across the tropical Pacific Ocean (McPhaden et al. 1998) (Fig. 1). Additional buoys at 3.5°, 10°, and 12°N along 95°W were deployed in late 1999 as part of the Pan American Climate Studies (PACS) program. PIRATA is an array of 12 ATLAS buoys in the tropical Atlantic (Servain et al. 1998). Currently, 28 ATLAS moorings in the TAO/TRITON array have self-siphoning rain gauges, while all PIRATA ATLAS moorings are equipped with such gauges.

Data from these buoy programs have potential widespread application in research related to climate variability and ocean–atmosphere interaction. The accuracy of datasets from these programs is therefore an issue of significant importance, and previous reports describing error characteristics for winds, air temperatures, relative humidity, ocean temperatures, ocean salinities, and currents have already appeared in the literature (Plimpton et al. 1997; Freitag et al. 1995, 1999; Freitag et al. 2001, manuscript submitted to *J. Atmos. Oceanic Technol.*). This study is the first systematic evaluation of the performance of the R. M. Young self-siphoning rain gauge on ATLAS moorings.

The purpose of this report is to quantify the errors in the ATLAS precipitation measurements. Errors in rain gauge measurements are related to both sensor accuracy and environmental conditions. We will use the manufacturer specifications, calibrations done at the National Oceanic and Atmospheric Administration (NOAA) Pacific Marine Environmental Laboratory (PMEL), and data from the field to assess these errors. Effects of environmental conditions such as wind speed, sea state, and evaporation will be discussed, and corrections for wind speed–dependent errors will be suggested based on results of previous studies. However, determining wind speed corrections specifically designed for the R. M. Young gauges is beyond the scope of this study.

2. Instrumentation

ATLAS buoys are designed and assembled at NOAA PMEL for the TAO/TRITON and PIRATA arrays. Standard ATLAS measurements include 3-m air temperature and relative humidity, 4-m wind speed and direction, and ocean temperatures at 11 depths from 1 to 500 m. New next-generation ATLAS buoys can additionally measure shortwave radiation, precipitation, and salinity, both at the surface (1 m) and below.

The next-generation ATLAS buoys measure precip-

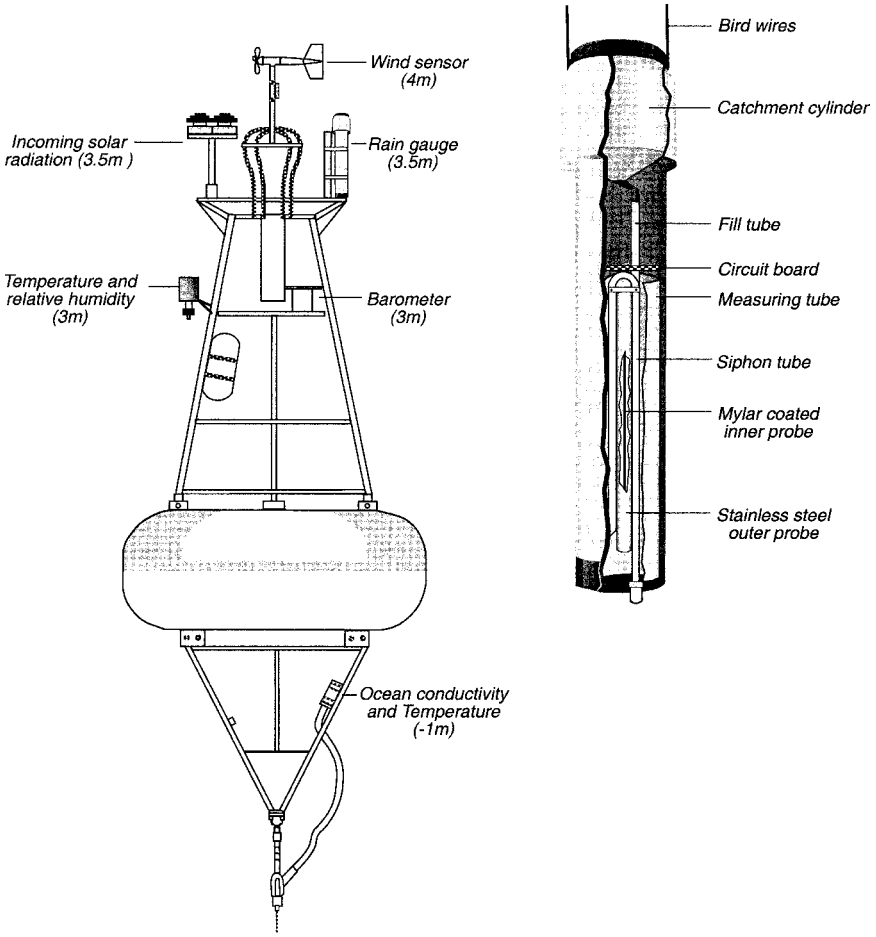

FIG. 2. Schematic of R. M. Young self-siphoning rain gauge model 50202/50203 and the ATLAS buoy with surface instrumentation noted.

itation using R. M. Young Model 50203-34 self-siphoning rain gauges (hereafter referred to as rain gauges or simply gauges) mounted 3.5 m above the ocean surface. The instruments have a 100-cm^2 (11.3-cm diameter) catchment cylinder mounted on top of a fill tube. Rainwater is captured by the upper cylinder and funneled into a cylindrical measuring tube below via the fill tube. Gauges are modified at PMEL to reduce power requirements and to digitize the analog output. A schematic of the rain gauge and its placement on the ATLAS buoy is provided in Fig. 2.

The measuring tube has a maximum capacity of 500 mL, equivalent to 50 mm of rain between siphon events. The volume of water in the tube is determined by capacitance. A stainless steel capacitive probe covered with mylar is located at the center of the measuring tube. The capacitance is measured between the steel probe and the water, with the mylar acting as the dielectric between these two ''plates'' of the capacitor. An outer stainless steel probe surrounding the inner mylar coated probe closes the circuit. As the water level rises, increasing the surface area in touch with the mylar, the capacitance increases.

A PMEL-designed circuit converts the capacitance to frequency, which is then averaged over 1-min intervals and output as a digital signal (counts). The conversion from counts to volume is given by the equation

$$V = \frac{a}{N} + b, \tag{1}$$

where V (in mL) is the volume in the measuring tube, N is the number of counts, and a (in mL-counts) and b (in mL) are calibration coefficients to be determined through a least squares regression of V on N^{-1}. Mean coefficients for over 100 sensor calibrations are $a = 6.5 \times 10^7$ and $b = -1100$. The 1-min volume samples are stored on board the mooring while at sea, and are available for postprocessing on recovery.

While the mooring is deployed, the daily mean and standard deviation of rain rate, and the daily percent time raining, are sent to PMEL in real time via Service Argos, Inc., which makes use of NOAA polar orbiting

TABLE 1. Data used for this study. Also see Fig. 1 for a chart of locations.

Location	Deployment no.	Deployment start date	Deployment end date	No. of days with data
13°N, 114°E	043a	98-04-13	98-12-24	242
18°N, 116°E	020a	97-04-17	97-06-12	56
	098a	99-08-20	00-05-06	260
8°N, 165°E	023a	97-06-10	98-01-04	166
	093a	99-08-06	00-07-18	312
5°N, 165°E	024a	97-06-11	98-01-05	187
	024b	98-01-06	98-07-08	164
	052a	98-07-09	99-08-06	37
	094a	99-08-08	00-02-12	156
	094b	00-02-24	00-07-19	74
2°N, 165°E	032a	98-01-07	98-03-12	22
	032b	98-07-10	99-03-20	253
	095a	99-08-09	00-02-27	161
	130a	00-02-28	00-04-20	52
0°, 165°E	033a	98-01-08	98-07-10	164
	081a	99-03-20	99-06-20	92
	081b	99-06-20	99-08-10	51
	131a	00-02-29	00-07-22	144
2°S, 165°E	025a	97-06-15	98-01-09	208
	054a	98-07-12	99-03-14	127
	054b	99-03-14	99-05-18	28
	097a	99-08-12	00-02-26	55
5°S, 165°E	034a	98-01-11	98-07-13	91
	080a	99-03-14	99-08-13	152
	080c	99-10-20	00-03-01	133
8°S, 165°E	026a	97-06-17	98-07-14	352
	055a	98-07-14	99-03-12	241
	079a	99-03-13	99-08-13	153
	079b	99-08-14	00-05-11	189
8°N, 167°E	092a	99-07-30	99-09-13	45
8°N, 168°E	091a	99-07-29	99-09-14	47
5°N, 140°W	069a	99-02-01	99-09-17	228
	069b	99-09-17	00-02-09	145
2°N 140°W	103a	99-09-19	00-02-11	145
0°, 140°W	047a	98-05-11	98-09-21	120
	072a	99-02-05	99-09-19	226
	104a	99-09-21	00-02-12	144
8°N, 125°W	016b	97-08-08	97-10-04	47
	016c	97-10-05	98-04-24	187
0°, 125°W	018b	97-10-09	98-04-18	107
	046a	98-04-29	98-09-18	140
	058a	98-09-18	99-02-12	147
	058b	99-02-12	99-10-01	231
	105a	99-10-02	00-02-21	142
8°N, 110°W	029b	98-03-06	98-10-22	207
0°, 110°W	083a	99-05-12	99-11-15	187
	114a	99-11-16	00-05-07	173
10°N, 95°W	122a	99-12-02	00-04-21	141
8°N, 95°W	028a	97-08-06	98-02-03	154
	028b	98-02-15	98-07-25	85
	121a	99-12-01	00-04-22	118
5°N, 95°W	087a	99-05-26	99-11-29	187
	087b	99-11-29	00-04-23	146
4°N, 95°W	120a	99-11-29	00-04-24	147
2°N, 95°W	118a	99-11-28	00-04-25	149
0°, 95°W	064a	98-11-07	99-05-22	196
	085a	99-05-23	99-11-26	168
	117a	99-11-27	00-04-26	151
2°S, 95°W	116a	99-11-26	00-04-27	84
8°S, 95°W	115a	99-11-24	00-04-29	157
15°N, 38°W	036a	98-01-28	99-02-05	373
	073a	99-02-06	00-03-14	402
12°N, 38°W	070a	99-02-03	00-03-16	407
8°N, 38°W	037a	98-01-30	99-01-28	352
	074a	99-02-09	99-08-01	21

TABLE 1. (*Continued*)

Location	Deployment no.	Deployment start date	Deployment end date	No. of days with data
0°, 35°W	035a	98-01-22	99-02-16	382
	077a	99-02-23	99-07-23	29
	077b	99-07-23	00-03-28	249
0°, 23°W	078a	99-03-06	99-08-04	151
	078b	99-08-04	00-02-23	203
2°N, 10°W	111a	99-11-03	00-01-26	84
0°, 10°W	068a	99-01-29	99-08-16	159
	068b	99-08-16	99-11-02	78
	068c	99-11-02	00-01-21	80
2°S, 10°W	110a	99-11-02	00-03-12	118
5°S, 10°W	067a	99-01-27	99-08-13	109
	067c	99-11-01	00-03-13	133
0°, 0°	066a	98-11-08	99-01-11	53

Total number of days with data = 12 346.

weather satellites for data telemetry. The daily rates R are calculated in units of millimeters per hour based on 1-min rates using,

$$R = \left(\frac{aK}{c}\right)\frac{\text{mL}}{\text{min}} \times 0.1\,\frac{\text{mm}}{\text{mL}} \times 60\,\frac{\text{min}}{\text{h}}, \qquad (2)$$

where K is defined by

$$K = \frac{1}{M}\sum_{i=1}\left(\frac{1}{N_i} - \frac{1}{N_{i+1}}\right)c, \qquad (3)$$

a is the slope from Eq. (1), and M is the number of 1-min samples collected in the 24-h period (typically 1440). Equation (3) is scaled by c in order that K be transmitted as a 16-bit integer. The scale factor c is 2^{32}. The percent time raining is calculated using a 1 mm h^{-1} threshold to indicate rain events.

Conversion from volumes to accumulations requires removing siphon events. A siphon event occurs when the gauge reaches its maximum capacity of 500 mL, at which time water is expelled from the measuring tube through a siphon tube. Siphoning occurs over about a 30-s period and is identified as sharp decreases in volume. In real time one or two data points are identified as a siphon event (equivalent to 1–2 min of data) and are ignored when calculating the daily statistics. In postdeployment processing, data associated with siphon events are flagged, typically removing 3 min worth of data centered on the event.

Once the mooring is recovered, the 1-min accumulations are first flagged for obviously erroneous data. A 16-min Hanning filter is then applied to these data to generate smoothed 10-min accumulations. Rates are calculated by differencing the 10-min data and converting to mm h^{-1}. The daily statistics are recomputed based on the 10-min rates, continuing to use a 1 mm h^{-1} threshold to calculate percent time raining.

Differentiating Eq. (1) with respect to N, the resolution of the volume data is given by

$$\frac{dV}{dN} = \frac{-a}{N^2}. \qquad (4)$$

Equation (4) indicates that resolution is dependent on counts, and increases with fullness of the measuring tube. Typical counts for empty and full tubes are 59 090 and 40 625, respectively, giving a range of resolution for the 1-min volumes of 0.02–0.04 ml, equivalent to 0.2–0.3 mm h^{-1} for 1-min rates.

The resolution of the real-time daily rates is found from differentiating Eq. (2) with respect to K, giving

$$\frac{dR}{dK} = 6\frac{a}{c}. \qquad (5)$$

This is equivalent to 0.09 mm h^{-1} for $a = 6.5 \times 10^7$.

A large portion of the data used for the current study have been collected with the version 1 circuitry described by Eqs. (1)–(5). Starting in late 1999, version 2 circuit boards replaced version 1 boards in the field. The calibration equation for version 2 boards is

$$V = \frac{a}{N^2} + b, \qquad (6)$$

where the variables have the same definition as in Eq. (1). The mean calibration coefficients are $a = 1.3 \times 10^{12}$ and $b = 440$, based on 24 sensor calibrations. For these calibrations, typical values of N when empty and full are 53 700 and 37 000, respectively.

The real-time daily rates are calculated using Eq. (2), where K is now given by

$$K = \frac{1}{M}\sum_{m=1}^{M}\left(\frac{1}{N_m^2} - \frac{1}{N_{m+1}^2}\right)c, \qquad (7)$$

and the scale factor c is 2^{47}. Calculation of the real-time daily statistics and postprocessing are done in a the same manner as for the version 1 data.

The 1-min volume resolution for the version 2 boards is found by differentiating Eq. (6) to give

TABLE 2. Summary of laboratory experiments documenting instrument noise when raining. Std devs (σ) represent instrument noise and, to a lesser degree, pump noise about the mean pump rates indicated in column 3. Std devs below the expected errors in pump accuracy are in bold. Only 1 out of 13 experiments have σ's below the expected pump error for 1-min data, and 4 out of 13 experiments have σ's below the expected pump error for 10-min data. Std devs excluding siphon events are several times lower than those surrounding siphon events. As siphon events are infrequent, these errors are not included in estimates of the self-siphoning rain gauge instrument noise.

				1-min rates		10-min rates	
Serial no.–version no.	Expt. no.	Pump rate (mm h^{-1}) ± 1%	No. of siphon events	σ (no siphons) (mm h^{-1})	σ (±10 min of siphons) (mm h^{-1})	σ (no siphons) (mm h^{-1})	σ (±10 min of siphons) (mm h^{-1})
744–1	1	4.70 ± 0.05	2	2	5	0.9	2
	2	8.70 ± 0.09	18	1	6	0.4	1
	3	9.00 ± 0.09	11	1	7	0.6	1
	4	128 ± 1	40	**1**	12	**0.6**	3
618–1	5	10.5 ± 0.1	8	0.7	5	0.2	3
	6	53.2 ± 0.5	21	2	7	**0.3**	2
707–1	7	10.5 ± 0.1	8	0.6	5	0.2	3
	8	53.1 ± 0.5	25	2	10	**0.5**	2
670–1	9	10.5 ± 0.1	5	1	4	0.6	1
679–2	10	10.8 ± 0.1	5	0.5	6	0.2	2
709–2	11	10.7 ± 0.1	13	1	4	0.2	1
	12	55.3 ± 0.5	25	3	6	**0.4**	2
755–2	13	10.7 ± 0.1	8	0.6	6	0.2	1
Meanσ				1.3	6	0.4	1.8

$$\frac{dV}{dN} = \frac{-2a}{N^3}. \tag{8}$$

Using the mean calibration slope a and typical values for counts N for these boards, the resolution ranges from 0.02 to 0.05 mL, for an empty to full measuring tube, respectively, equivalent to 0.12–0.3 mm h^{-1} for the 1-min rates. Using Eq. (5) with the newer value for a and the scale factor c, the real-time daily resolution is 0.06 mm h^{-1}, compared with 0.09 mm h^{-1} for version 1.

Version 2 circuitry enhances resolution and is also designed to reduce noise related to radio frequency energy. However, the newer circuitry does not differ significantly from version 1 with respect to the errors discussed in this study, except where stated explicitly. Version 1 boards are no longer in use on the moorings.

3. Methodology

Table 1 summarizes the locations, deployments, deployment dates, and number of days with observations for the rain gauge data used in this study. A total of 78 deployments from 36 different locations are included in the analysis. Of the 78 deployments, 12 have version 2 circuitry. The number of days with observations are not necessarily equivalent to the length of the deployment because of missing or flagged data. For the deployments shown in Table 1, 75% of the deployments have 83% or better data recovery, and 50% have a 100% data recovery. In total, over 12 000 days of 1-min samples have been analyzed.

While analysis of the field data provides some estimate of instrument noise, it is not possible to unambiguously separate signal from noise during rainy periods. Because rain rate is not a smoothly varying quantity, it is difficult to define a reliable mean and corresponding variance, which would represent noise, and not also include the natural variability of rain. Thus, we include data from 13 laboratory experiments in this study in order to investigate instrument noise during active accumulation. The experiments varied from 23–70 h in length, during which time a pump delivered constant, known amounts of water to the gauge. A total of seven different rain gauges were tested using a range of pump rates nominally from 5–125 mm h^{-1}, accurate to 1%. The raw, 1-min volumes were processed in the same way as the buoy data, thus permitting an analysis of both instrument performance and PMEL processing procedures. The results of these experiments are summarized in Table 2.

4. Nominal sensor accuracy

R. M. Young specifies their sensor accuracy at 1 mm. Yuter and Parker (2001) use an accuracy of 0.5 mm for the R. M. Young rain gauges in their study. Calibration at PMEL of over 100 version 1 rain gauges from counts to volumes using Eq. (1) indicates accuracies of 0.3 mm. Calibration slopes a are repeatable with an 0.2% root-mean-square (rms) error, and rms offsets b are 0.3 mm, based on 12 repeats. A 0.2% error in the slope is equivalent to errors on the order of 0.05 mm in volume. Precalibration minus postcalibration slope differences have an rms error of 1%, based on 22 pre-/postdeployment pairs, equivalent to accumulations of tens of millimeters over a 6-month deployment period. Pre- minus postcalibration rms offsets are 2.4 mm. Note that offsets

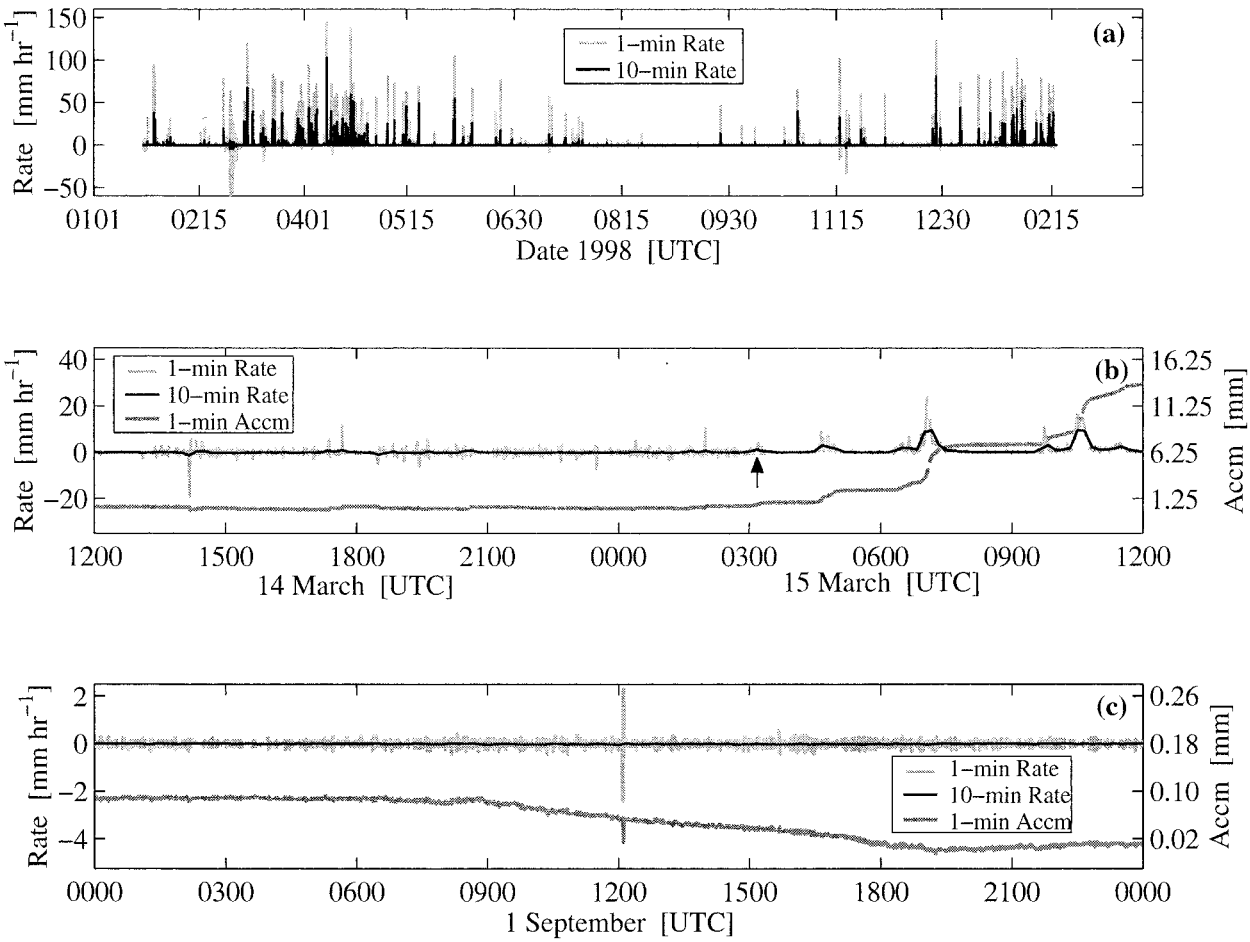

FIG. 3. Example of rain gauge data from 0°, 35°W. (a) 1- and 10-min rain rates. Time axis is in mmdd format, where mm is month and dd is day. (b) Same as (a) but for 14–15 Mar 1998 and includes 1-min accumulations. Arrow indicates time of siphon event. (c) Same as in (b) but for 1 Sep 1998. Time axis is in hhmm format for panels (b) and (c), where hh is hour and mm is minute.

do not affect rain-rate calculations. Calibration of 24 version 2 self-siphoning rain gauges at PMEL indicates similar calibration accuracies to those of the version 1 gauges.

The accuracy of the calibration also gives an idea as to the expected noise level for the instrument. Noise in volume measurements of 0.3 mm, if treated as independent and random, is equivalent to errors of ± 30 mm h^{-1} for 1-min rain rates, or ± 3 mm h^{-1} for unsmoothed, 10-min rates. However, errors in volume tend to be correlated, such that adjacent volume measurements are offset from the calibrated values in the same direction, making the error in their difference typically much less than 0.3 mm. This is consistent with visual inspection of the rain-rate data, which does not indicate that noise on the order of the calibration errors is a common occurrence. Thus, it can be misleading to simply use calibration errors for volume to estimate errors in rain rates. Instead, we adopt more direct error estimation procedures for rain rate as discussed below.

5. Estimation of rain-rate errors

A typical example of the rain gauge data is provided by the 1998 deployment at 0°, 35°W in the tropical Atlantic shown in Fig. 3. Figure 3a shows 1- and 10-min rain rates for the entire deployment, while Figs. 3b and 3c show subsamples of these data for two 24-h periods. The first is from 14–15 March 1998 (Fig. 3b), a period of frequent rain events, and the second is from 1 September 1998 (Fig. 3c), a period with no rain events. Figures 3b and 3c also show 1-min accumulations. These data indicate the discontinuous nature of rainfall variability and the consequent challenge of distinguishing signal from noise.

Despite the overall irregularity of the time series, some measure of instrument performance is discernible from these data. For example, the noise of the instrument is observed as small fluctuations about zero on the order of 1 mm h^{-1} or less, with the smallest amplitudes observed during dry periods, like that shown in Fig. 3c.

TABLE 3. Summary of errors. Dry period errors are empirically determined from rain gauge data collected by buoys highlighted in Fig. 1. Rainy period errors are determined from laboratory experiments detailed in Table 2.

Error description	1-min	10-min	Comments
R. M. Young specifications	85 mm h^{-1}	8 mm h^{-1}	Assumes independent random error based on 1-mm accuracy in 1-min accumulations.
PMEL calibrations	30 mm h^{-1}	3 mm h^{-1}	Assumes independent random error based on 0.3-mm accuracy found for 1-min accumulations.
Instrument noise: no rain present	0.3 mm h^{-1}	0.1 mm h^{-1}	Empirically determined noise standard deviation based on dry periods in field data.
Instrument noise: rain present	1.3 mm h^{-1}	0.4 mm h^{-1}	Empirically determined noise standard deviation based on PMEL lab data not including siphon events.
Evaporation	Negligible to 0.2 mm day^{-1}		Site dependent.
Suggested overall error			
No rain present	0.3 mm h^{-1}	0.1 mm h^{-1}	
Rain present	1.3 mm h^{-1}	0.4 mm h^{-1}	

It is also seen that significant negative rates, indicative of random noise, are episodic in nature, and tend to occur more often during periods with significant rainfall. An example of such noise is observed at 1424 UTC 14 March (Fig. 3b), when a decrease in the volume measurement results in a -20 mm h^{-1} (-2 mm h^{-1}) rate in the 1-min (10-min) data. Noise of this nature also occurs during periods of little or no significant rainfall, such as that observed near 1200 UTC 1 September (Fig. 3c). In this case a single erroneous volume measurement causes one positive and one negative spike of 2 mm h^{-1} in the 1-min data, an order of magnitude less than that observed during the period of significant rainfall. This difference in magnitude between noise during rainy and dry periods is typical of the data analyzed in this study and is discussed further in sections 5a–d.

Also evident in Fig. 3c is a decrease in accumulation throughout the day, where local time is back 2 h from the UTC times shown. The net accumulation over the 24-h period is -0.07 mm and is attributed to evaporation from the measuring tube. This difference is somewhat less than the maximum difference in accumulation over this same 24-h period, due to a slight increase in accumulation following the daily minimum reading at about 1900 UTC. Diurnal fluctuations, caused by the sensitivity of the circuitry to temperature, are frequently observed under fair weather conditions. The amplitude of the diurnal variability is 0.02 mm in this example, with readings highest at predawn, when the ambient temperature is at a minimum.

The remainder of this section describes the behavior of the rain gauges in more detail and quantifies the associated noise where possible. A summary of identified errors and suggested overall instrument errors is provided in Table 3.

a. Dry period noise

To compare the variability observed in the 1- and 10-min rate data to the instrument errors derived from PMEL calibrations presented in section 4, we identify dry periods in the data and use them to determine the standard deviation and range of values of the observations. Dry periods are identified as 20-min periods with no more than one value between 1.5 and 30 mm h^{-1} for the 1-min data, or between 0.5 and 3 mm h^{-1} for the 10-min data. Assuming no flagged data points, a total of 21 points are used to determine if a 1-min data point is dry, whereas a total of 3 data points are used to determine if a 10-min data point is dry. Because the 10-min data are determined from 16-min Hanning filtered 1-min accumulation data, we are technically including somewhat more than 20 min worth of information when determining dry periods for the 10-min data. The upper limits for determining dry periods are set by the PMEL calibration error estimates, while the lower limits are set by the standard deviation of laboratory data, to be presented in section 5d. Only one positive spike on the order of the calibration error is permitted within the 20-min window, but any number of negative spikes of unlimited magnitude may be present. The method inevitably captures some true rain events, but also provides a means for determining the variability of the field data.

The dry periods for all the deployments used in this study were combined and means and standard deviations were computed, giving 0.0 ± 0.3 mm h^{-1} for the 1-min data, and 0.0 ± 0.1 mm h^{-1} for the 10-min data. The 5th and 95th percentiles of these data were also calculated, the results of which indicate that 90% of the dry data lie between ± 0.4 mm h^{-1} for the 1-min data, and between ± 0.09 mm h^{-1} for the 10-min data. The standard deviation for the 10-min data is an order of magnitude larger than the 33d and 66th percentiles for these data of ± 0.01 mm h^{-1}, because of a relatively small number of large negative values skewing the calculation of the standard deviation. For this reason, the 5th and 95th percentiles of ± 0.09 mm h^{-1} lie inside of the range defined by the standard deviation. The standard deviations and the range of values for the 1- and 10-min field data lie well below the instrument error derived from PMEL calibrations.

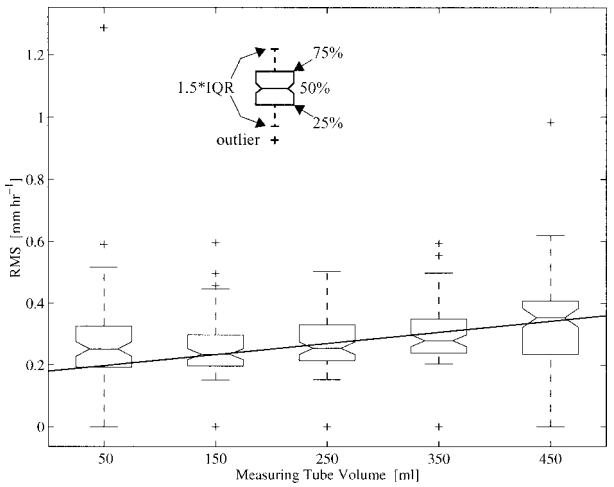

FIG. 4. Box plot of rms errors within volume bins using 1-min data from dry periods only. Each deployment provides an rms value for each bin, giving 78 rms values per bin. Volumes represent the center value of 100-mL-width bins. A schematic describes how to interpret the boxes. The line represents the resolution in rain rate based on the volume resolution of version 1 gauges as defined by Eq. (4).

b. Dependence on volume

Noise exceeding the typical standard deviation in the 1-min data for dry periods, though generally less than 1 mm h^{-1}, is sometimes observed when the collection tube is nearly full. Figure 3b shows an example of this behavior for the gauge at 0°, 35°W. Data in the first part of Fig. 3b indicates a higher amount of noise about zero than in Fig. 3c (note scale difference). The sudden reduction in this noise at 0311 UTC 15 March immediately follows a siphon event, indicating that noise was high when the measuring tube was near full. Visual inspection of the field data indicates that noise is often high when the measuring tube is full. Lab data indicate that noise can also be greater at other instrument-dependent volume levels, particularly at low levels.

To determine any dependence of noise on tube volume, 1-min rates for dry periods only are binned according to tube volume at 100-mL intervals, up to 500 ml. The rms error for each bin is then calculated, giving a total of 78 rms values per bin, one for each deployment. Selected statistics of the rms values for the bins are shown in Fig. 4 using notched box plots [described more fully in, e.g., Vellman and Hoaglin (1981)]. The upper, middle, and lower horizontal lines of the box represent the 75th percentile, median, and 25th percentile of the rms values within the bin, respectively. Thus, the size of the box represents the interquartile range (IQR) of the data. The width of the notches in the box estimate how well the median is known at the 95% confidence level, so that median values whose notches do not overlap are considered to differ significantly. The dashed lines extending from the box represent 1.5 times the IQR of the data. Finally, the plus symbols indicate outliers, where outliers are defined as data exceeding the median value by 1.5 times the IQR.

The box plots indicate that the mean rms error is greatest for the largest volume bin (400–500 mL), consistent with what is typically observed during processing. It is also apparent that the smallest volume bin has a large range of rms errors. The difference between the median rms error of the largest (400–500 mL) and smallest (0–100 mL) volume bins indicates that the sensitivity of the measurement to measuring tube volume may account for up to 0.1 mm h^{-1} differences in the noise level for 1-min rates. This type of noise is generally filtered out of the 10-min data during processing.

A possible explanation for the sensitivity of the measurement to measuring tube volume is related to the circuit design of the rain gauges. Equation (1) implies that the tube volume resolution is inversely related to counts. This results in a decrease in resolution with increasing volume, as is seen in Eq. (4). Therefore, at large volumes, a discrepancy in the number of counts leads to greater errors in the recorded volumes, and thus in the derived rain rates. The line shown in Fig. 4 represents the expected resolution in rain rate as a function of measuring tube volume based on Eq. (4). This equation is applicable to version 1 boards, which is relevant to most of the data analyzed in this study. Similar noise is observed with the version 2 boards, but the resolution as a function of volume would be calculated from Eq. (8) instead of (4). Overall, the observed rms noise is seen to increase with measuring tube volume, with median values matching the expected resolution in rain rate. However, significantly greater rms noise is observed at low tube volumes. In addition, the range of rms noise at both low and high tube volumes is greater than at intermediate tube volumes. Noise at low and high tube volumes is found to be attributed to siphon events and is discussed in more detail in section 5d.

c. Temperature sensitivity

A small but measurable error is associated with the dependence of the gauge circuitry on temperature. In general, larger volumes are seen for cooler nighttime temperatures. Transitions typically occur over the course of an hour or so at sunrise to smaller daytime volumes, with the situation reversed at sunset. Figure 5 shows this behavior over about a 10-day period at 0°, 35°W, along with the corresponding surface air temperature from the buoy for comparison. The dependence of volume on temperature is seen as diurnal fluctuations corresponding to changes in ambient air temperature. Evaporation is also evident as a linear decrease in accumulation over the 10-day period.

To estimate the temperature sensitivity, 24-h periods of 1-min volumes with rates less than 1.5 mm h^{-1}, and 10-min derived volumes with rates less than 0.5 mm h^{-1}, are analyzed. The mean diurnal difference for these data is calculated as the difference between the maxi-

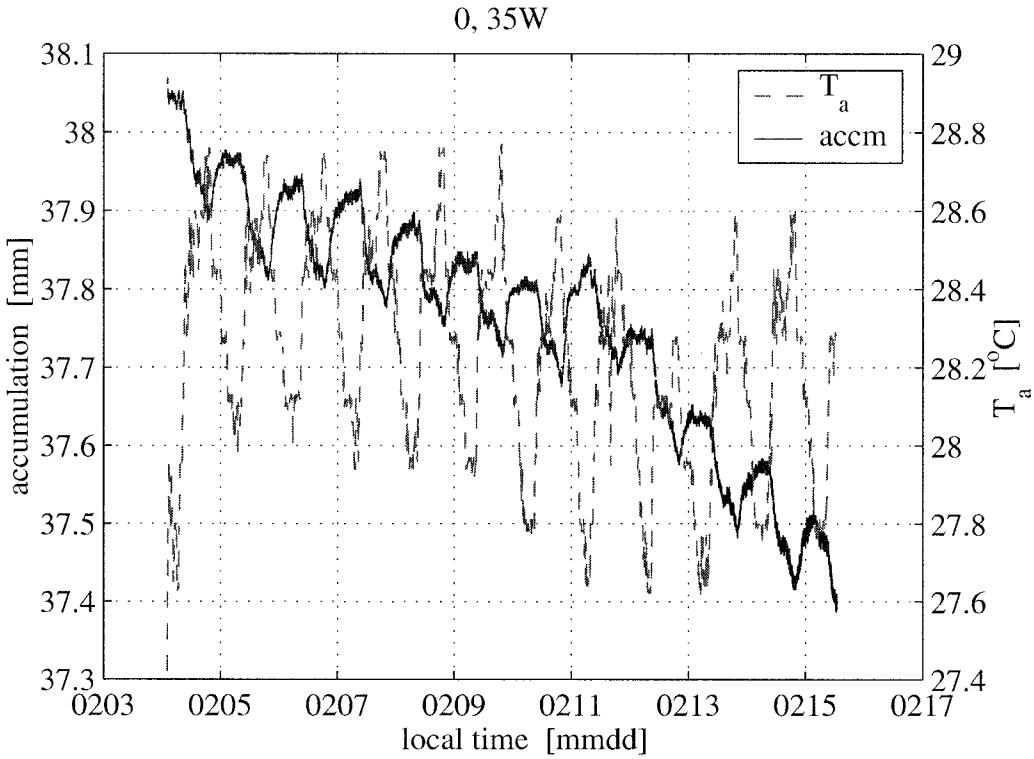

FIG. 5. Example of the diurnal signal in accumulation caused by sensitivity of the rain gauge circuitry to temperature. Evaporation is also evident over this 14-day time period. Time is shown in mmdd format. The solid line is 1-min accumulation (accm); the dashed line is 10-min air temperature (T_a).

mum difference in accumulation over the day, less the absolute value of the net accumulation over the same 24-h period. The average difference between daytime and nighttime volumes is −0.1 mm for the 1-min data, and −0.06 mm for the 10-min data. These differences amount to errors in rate on the order of hundredths of millimeters per hour for both 10- and 1-min data for typical circuit thermal response times of a few hours.

Volumes often read high during rain events, stabilizing to somewhat lesser values soon afterward. Decreases in accumulation are on the order of a few tenths of a millimeter over the stabilizing period, which is on the order of minutes to hours. It is postulated that the sensitivity of the circuitry to temperature may be responsible for this behavior, due to the proximity of the circuitry to the fill tube. If it is assumed that the rain is colder than the ambient air, the increase in volume is consistent with the sense of the diurnal cycle variability. A stabilization time period of minutes to hours might be expected, depending on the amount of new rainfall and the amount of rain in the gauge at the time. Spurious decreases in accumulation of this nature contribute to incidences of negative rain rates, more commonly observed in the 1-min data because the 1-min sampling fully resolves the stabilizing period. If these periods are longer than 10 min, negative rates will also be found in the 10-min data.

d. Laboratory results

As described in section 5a, the variance in rain rate during periods of little or no rain is found to be significantly less than the manufacturer or calibration errors provided in section 4. It is also of interest to know the behavior of the instrument during periods of significant rain. To address this issue laboratory experiments were performed, where a constant known flow rate was applied to a rain gauge with a mechanical pump accurate to 1%, as described in section 3. The results of these experiments are summarized in Table 2.

Higher noise levels are primarily the result of deviations from linear behavior assumed in the conversion from counts to volumes, as defined in Eq. (1). Contributing factors to this nonlinear behavior, such as volume and temperature dependencies, have already been discussed in sections 5b and 5c. This nonlinear behavior is most evident surrounding siphon events, as shown in Fig. 6, using the data from experiment 3 (Table 2). The upper panel shows 1- and 10-min rates and 1-min volumes. The lower panel shows a closer view of the rates and volumes for the period surrounding the siphon event at ~2000 UTC. The volume readings do not increase linearly for the relatively constant flow rate of 9 mm h^{-1}. Large deviations in the 1-min rates, and smaller but still significant deviations in the 10-min rates, are

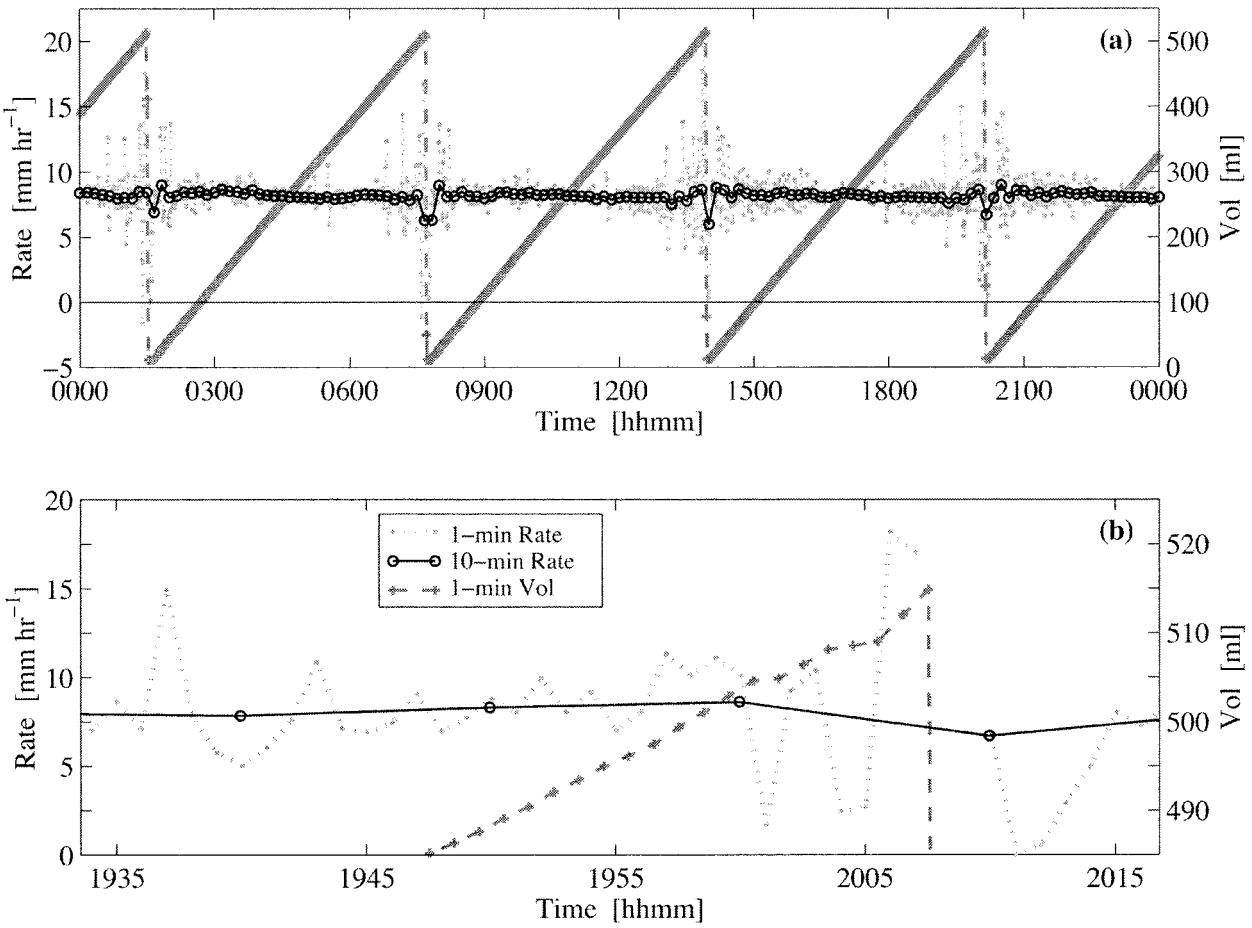

FIG. 6. (a) Rate and volume data for a 24-h period from expt 3. (b) Same as in (a) but for 40-min period surrounding siphon event at about 2000 UTC. Data indicates noise observed surrounding siphon events. Legend applies to both panels.

observed. The additional volume dependent noise at low and high tube volumes identified in the field data during dry periods (section 5c, Fig. 4) possibly results from this behavior.

The noise standard deviations excluding siphon events are consistently higher for both the 1- and 10-min data than their respective dry period standard deviations of 0.3 and 0.1 mm h^{-1}. Some of this error can be attributed to the pump, though in most cases the noise variance of the gauge exceeds the noise variance of the pump. Experiments where the noise variance of the gauge is equal to or less than that of the pump variance are in bold type in Table 2. The average noise standard deviation of the lab data, excluding ± 10 min of the siphon events, is 1.3 mm h^{-1} for the 1-min data and 0.4 mm h^{-1} for the 10-min data. The average noise standard deviation of the data around siphon events is 6 and 1.8 mm hr^{-1} for the 1- and 10-min data, respectively. As siphons events take only about 30 s and amount to at most hundredths of a percent of the deployment period, error estimates for periods of active accumulation provided in Table 3 assume these errors are negligible.

Factors such as tube volume and circuit board temperature have been identified as contributing to noise in the data. The lab studies indicate that noise in general is larger in magnitude during rainy periods. It is likely that larger fluctuations in the factors that generate noise are occurring during rainy periods, resulting in increased noise amplitude in the gauge data during these times.

6. Evaporation and sea spray

Evaporation is evident in the data as a slow decrease in accumulation over time. The evaporation rate estimated from the data is anywhere from negligible to -0.2 mm day^{-1}, equivalent to about 6 mm in a month. The evaporation rate differs significantly depending on the location of the buoy. Little evaporation is expected for these rain gauges, given the protection of the water surface from wind and direct sunlight. As seen in the schematic in Fig. 2, the measuring tube is contained inside the instrument, protected from direct sunlight and winds, minimizing loss due to evaporation from the water surface.

A slow increase in accumulation is also observed at times when presumably there is no rain, but to a lesser

degree than evaporation. This may be due either to sea spray or electronic drift of some sensors. While sea spray contamination can be quite substantial for gauges on a moving ship (e.g., Skaar 1955), these corrections should be much smaller for gauges on a buoy, which are not exposed to spray from a ship's hull. To estimate possible sea spray contamination, time periods with relatively high wind speeds and no rain were analyzed. An extreme case was a 25-day sample of data with an average wind speed of 8 m s^{-1} and no rain events. For this 25-day sample an accumulation of 0.01 mm day^{-1} was observed. Overall, the daily accumulations from this time period show little or no dependence on wind speed, indicating no obvious sea spray contamination.

Preobrazhenskii (1973) provides field estimates of water content at several heights above the sea surface based on data collected from a boom extended from the bow of a ship in the North Atlantic. At 4 m above sea level, the approximate height of the ATLAS rain gauges, their estimates are 2×10^{-5} g m^{-3} for 7 – 12 m s^{-1} winds, and 2×10^{-3} g m^{-3} for 15 – 25 m s^{-1} winds. For a buoy tilted 10° into a 25 m s^{-1} wind, sea spray concentrations of 2×10^{-3} g m^{-3} amount to salt water accumulation rates of 0.03 mm h^{-1}. This is a ''worst case'' estimate of sea spray contamination, as it assumes that all spray enters the gauge, and that the buoy is tilted into the wind. In practice, much of the flow would be deflected away from the gauge orifice, and the buoy would be tilted into the wind only a fraction of the time.

7. Wind

Despite the longtime use of catchment-type rain gauges, few studies are available that quantify the error induced by wind on rain gauge collection efficiency. An early study by Koschmieder (1934) compared three rain gauges at about 1 m above the ground to a sunken Hellmann rain gauge. The aboveground gauges had diameters ranging from 16.0 to 25.2 cm, and the sunken Hellmann gauge had a diameter of 16.0 cm. Results from this study suggest undercatch of 10% for wind speeds of 4 m s^{-1}, 50% for 12 m s^{-1} winds, and 70% for winds of 16 m s^{-1}.

In a similar study three standard rain gauges mounted on a tower 34 m above the surface were calibrated against a ground catchment, the results of which are summarized in the World Meteorological Organization Technical Note No. 47 (World Meteorological Organization 1962), addressing measurement of precipitation from ships. The results suggest losses of 0%–19% for wind speeds <5 m s^{-1}, 15%–46% for 5–10 m s^{-1} winds, and 50%–83% for winds of 10–15 m s^{-1}, in agreement with the Koschmieder study. Yang et al (1998) estimate the wind speed correction for the standard National Weather Service gauge (National Weather Service 1989), catchment diameter of 20.3 cm, by comparing the performance of these gauges, both shielded and unshielded, to a double-fence comparison reference. Observed losses are similar to those observed by the other studies. Yuter and Parker (2001) use the results of Yang et al. (1998) to correct rain rates for their R. M. Young rain gauge data.

In a modeling study by Nešpor and Sevruk (1999), the turbulent flow around a cylinder is used to estimate gauge efficiency by comparing the volume of drops passing by the equivalent catchment surface area, with and without the presence of the cylinder to disturb the flow. Three gauges are modeled, one with a catchment diameter of 12.7 cm, and the other two with catchment diameters of 16.0 cm. Their study indicates that errors increase not only with higher wind speeds, but also with smaller drop sizes. For wind speeds 0–8 m s^{-1} they find 100% error for drop diameters <0.4 mm, 10%–50% error for drop diameters of 0.5 mm, and $<10\%$ error for diameters >1 mm. They also estimated the effect of rain rate on the wind induced errors. For 1–3 m s^{-1} winds errors are $<3\%$ for rates >2 mm h^{-1}, increasing exponentially for rates <1 mm h^{-1}. For wind speeds of 5–15 m s^{-1} errors are 1%–8% for rates >10 mm h^{-1}, 3%–11% for rates of 5 mm h^{-1}, and increase exponentially for rates <5 mm h^{-1}. Lighter rain events are likely to contain smaller drop sizes, compounding the wind induced errors.

For the ATLAS data, wind speeds less than 5 m s^{-1} occur 39% of the time, wind speeds of 5–10 m s^{-1} occur 59% of the time, and wind speeds in the range of 10–15 m s^{-1} occur the remaining 2% of the time. The frequency of wind speeds greater than 10 m s^{-1} increases with distance from the equator. According to the above studies, which are summarized in Table 4, undercatch of rain in these conditions is expected to be on the order of 10%–50%.

Using a correction scheme based on Koschmieder (1934), Bradley (1995) found agreement of better than 10% between mini ORG and corrected R. M. Young siphon gauge accumulated rainfall collected during TOGA COARE aboard the R/V *Franklin*. Based on this encouraging result, it may be possible to correct ATLAS rainfall measurements using ATLAS wind speed measurements, which are available at 10-min intervals. A third-order polynomial fit to the Koschmieder (1934) data yields

$$p(w) = -0.0141w^3 + 0.4409w^2 + 0.9927w + 0.1010, \quad (9)$$

where p represents the percent undercatchment at the given wind speed w. ATLAS rainfall data adjusted using 10-min winds in (9) may be an improvement over raw uncorrected rain data. As the R. M. Young gauges come into more widespread use, a correction specific to these gauges will hopefully be developed.

8. Summary and discussion

Analysis of the data from 78 R. M. Young self-siphoning rain gauges mounted on the next-generation

TABLE 4. Wind speed effects on funnel-type rain gauges found by various studies. Also shown are the frequencies of occurrence of wind speed ranges observed at the buoys.

Reference	Wind speed range	Comment
Buoy data used for this study	0–5 m s^{-1}	39% occurrence
	5–10 m s^{-1}	59% occurrence
	10–15 m s^{-1}	2% occurrence
Koschmieder (1934)	0–5 m s^{-1}	0%–12% undercatchment
	5–10 m s^{-1}	12%–40% undercatchment
	10–15 m s^{-1}	40%–67% undercatchment
World Meteorological Organization (1969)	0–5 m s^{-1}	0%–19% undercatchment
	5–10 m s^{-1}	15%–46% undercatchment
	10–15 m s^{-1}	50%–83% undercatchment
Yang et al. (1998)	5 m s^{-1}	20% undercatchment
Nešpor and Sevruk (1999) (model study)	0–8 m s^{-1}	100% undercatchment ($d < 0.4$ m), 10%–50% undercatchment ($d \sim 0.5$ mm), 10% undercatchment ($d > 1.0$ mm). d = diameter.
	1–3 m s^{-1}	<3% undercatchment ($R > 2$ mm h^{-1}), increases exponentially with decreasing R. R = rain rate.
	5–15 m s^{-1}	1%–8% undercatchment ($R > 10$ mm h^{-1}), 3%–11% undercatchment ($R \sim 5$ mm h^{-1}), increases exponentially with decreasing R.

ATLAS buoys suggests that these instruments exhibit fairly stable behavior in the field. Table 3 summarizes the sources and magnitude of noise identified in this study. Typical errors in the derived rain rates away from siphon events are on average 1.3 mm h^{-1} for the internally recorded 1-min data, and 0.4 mm h^{-1} for postprocessed 10-min data. Larger errors surround siphon events, averaging 6 mm h^{-1} in the 1-min data, and 1.8 mm h^{-1} in the 10-min data.

Evaporation from the rain gauges is observed to be at most 0.2 mm day^{-1}, or 6 mm in a month. Losses of this magnitude are within measurement error, and are therefore not generally a concern. Errors associated with sensor drift or sea spray are also found to be negligible.

Undercatch due to wind is expected to be the largest source of error for rain gauge measurements. Correction methodologies for wind-induced catchment errors are available in the literature (e.g., Koschmieder 1934), and have been found to improve the agreement between R. M. Young self-siphoning rain gauges and mini optical rain gauges (Bradley 1995). Table 4 summarizes catchment errors found in the literature as a function of wind speed. It is recommended that a correction for these errors, such as that provided in Eq. (9) based on Koschmieder (1934), be applied to the ATLAS self-siphoning rain gauge data for best estimates of the actual rain rates.

Discussion in this paper has focussed primarily on the internally recorded, postprocessed data from ATLAS moorings. However, it is also important to characterize the errors in the real-time daily averaged rain rate, since scientific analysis using the realtime daily averages often begins before moorings are recovered. Also, there are times when moorings are lost and no internally recorded data are retrieved.

To estimate the errors applicable to current software in the real-time daily rain rates, we consider two extreme limits, one in which it is assumed to be raining 100% of the time and one in which it is assumed to be raining 0% of the time. We further assume that the instrument noise will be reduced by $1/(N)^{1/2}$ where N (=1440) is the number of 1-min samples on which the daily averages are based. Errors related to siphon events are excluded in this calculation because these events occur, on average, less than once per day. The noise reduction assumption derives from the fact that errors in 10-min averages scale roughly as $1/(N)^{1/2}$ compared to the errors in 1-min estimates for both rainy and dry periods, as indicated in Table 3. Presumably, therefore, rain rate noise is random and uncorrelated from one minute to the next. For a 1-min standard error of 1.3 mm h^{-1} during rainy periods and 0.4 mm h^{-1} during dry periods, instrument error in daily averaged rain rates would be approximately 0.03 and 0.01 mm h^{-1}, respectively. For an intermediate situation in which it rained 10% of the day, the error would be 0.015 mm h^{-1}. Typical daily averaged rain rates recorded by ATLAS buoys range from a few tenths to a few millimeters per hour. Thus, expected rain rate errors due to random instrument noise are generally one to two orders of magnitude lower than the signals of interest. From this we conclude that instrument errors are not a limiting factor for determining realtime daily rain rates. As for the 1- and 10-min data, the most serious limitation on the accuracy of our real-time daily averages is likely to be the undercatch due to wind.

The bulk of the data used for this study were collected with rain gauges containing PMEL version 1 circuit boards. The latest rain gauges on ATLAS buoys contain

version 4 circuitry, which has the same logic as version 2 described in Eqs. (6)–(8). Version 2 and later circuit boards are designed to reduce sensitivity to radio frequency noise. Version 4 circuitry is additionally designed to reduce temperature sensitivity at temperatures below 20°C. Otherwise, there is no significant difference between the version 1 and later boards with respect to the noise characteristics discussed in this study.

We have indicated that the largest expected errors in the ATLAS rain gauge measurements are caused by the action of the wind on the gauge catchment efficiency. Determining a correction for wind speed effects could be done as either a laboratory or field experiment, but either would require substantial effort. A laboratory-based study would require a source of artificial rainfall with a realistic drop size distribution in an area where wind speed could be controlled. A field experiment like that of Koschmieder (1934) and others would require a reference gauge that is not affected by the action of the wind. Moreover, given the dependence of the wind speed correction on drop size distribution, the field experiment would have to be conducted in tropical rain conditions for it to be applicable to ATLAS mooring measurements. As with previous studies of this nature (e.g., Koschmieder 1934, Yang et al. 1998), a field experiment could take up to several years before enough data are collected to obtain stable statistics over the expected range of tropical rain rates and wind speeds. Thus, while we believe that a wind speed correction should be determined specifically for the R. M. Young gauges, development of such a correction is beyond the scope of this study.

Acknowledgments. The authors would like to thank Frank Bradley, Sandra Yuter, George Huffman, and Thomas Bell for helpful discussions regarding rainfall measurement during the course of this work. We would also like to thank George Huffman, Sandra Yuter, and three anonymous reviewers for their insightful comments on the first version of this manuscript. This work was supported by the NASA Tropical Rainfall Measuring Mission (TRMM) Science Program and the National Oceanic and Atmospheric Administration.

REFERENCES

Bradley, F., 1995: *Proc. of the Joint Workshop of the TOGA COARE Flux and Atmospheric Working Groups,* Boulder, CO, TCIPO, 35 pp.

Cronin, M. F., and M. J. McPhaden, 1998: Upper ocean salinity balance in the western equatorial Pacific. *J. Geophys. Res.,* **103,** 27 567–27 587.

Freitag, H. P., Y. Feng, L. J. Mangum, M. P. McPhaden, J. Neander, and L. D. Stratton, 1995: Calibration procedures and instrumental accuracy estimates of TAO temperature, relative humidity and radiation measurements. NOAA Tech. Memo. ERL PMEL-104, 32 pp.

——, M. E. McCarty, C. Nosse, R. Lukas, M. J. McPhaden, and M. F. Cronin, 1999: COARE Seacat data: Calibrations and quality control procedures. NOAA Tech. Memo. ERL PMEL-115, 89 pp.

Godfrey, J. S., R. A. Houze Jr., R. H. Johnson, R. Lukas, J.-L. Redelsperger, A. Sumi, and R. Weller, 1998: Coupled Ocean–Atmosphere Response Experiment (COARE): An interim report. *J. Geophys. Res.,* **103** (C7), 14 395–14 450.

Huffman, G. J., R. F. Adler, B. Rudolf, U. Schneider, and P. R. Keehn, 1995: Global precipitation estimates based on a technique for combining satellite-based estimates, rain gauge analysis, and NWP model precipitation information. *J. Climate,* **8,** 2810–2823.

Janowiak, J. E., and P. Xie, 1999: CAMS–OPI: A global satellite–rain gauge merged product for real-time precipitation monitoring applications. *J. Climate,* **12,** 3335–3342.

Koschmieder, H., 1934: Methods and results of definite rain measurements. *Mon. Wea. Rev.,* **62,** 5–7.

McPhaden, M. J., and Coauthors, 1998: The Tropical Ocean-Global Atmosphere observing system: A decade of progress. *J. Geophys. Res.,* **103,** 14 169–14 240.

National Weather Service, 1989: Cooperative station observations. NWS observing handbook No. 2, Silver Spring, MD, 83 pp.

Nešpor, V., and B. Sevruk, 1999: Estimation of wind-induced error of rainfall gauge measurements using a numerical simulation. *J. Atmos. Oceanic Technol.,* **16,** 450–464.

Plimpton, P. E., H. P. Freitag, and M. J. McPhaden, 1997: ADCP velocity errors from pelagic fish schooling around equatorial moorings. *J. Atmos. Oceanic Technol.,* **14,** 1212–1223.

Preobrazhenskii, L. Yu., 1973: Estimate of the content of spray-drops in the near-water layer of the atmosphere. *Fluid Mech. Sov. Res.,* **2,** 95–100.

Servain, J., A. J. Busalacchi, M. J. McPhaden, A. D. Moura, G. Reverdin, M. Vianna, and S. E. Zebiak, 1998: A pilot research moored array in the tropical Atlantic (PIRATA). *Bull. Amer. Meteor. Soc.,* **79,** 2019–2031.

Skaar, J., 1955: On the measurement of precipitation at sea. *Geofys. Publ.,* **19,** 1–32.

Thiele, O. W., M. J. McPhaden, and D. A. Short, 1995: Optical rain gauge performance. *Proc. of the Second Workshop on Optical Rain Gauge Measurements,* Greenbelt, MD, NASA, 76 pp.

Velleman, P. F., and D. C. Hoaglin, 1981: *Applications, Basics, and Computing of Exploratory Data Analysis.* Duxbury Press, 354 pp.

World Meteorological Organization, 1962: Precipitation measurements at sea. Tech. Note 47, WMO No. 124.TP.55, 18 pp.

Xie, P., and P. A. Arkin, 1997: Global precipitation: A 17-year monthly analysis based on gauge observations, satellite estimates, and numerical model outputs. *Bull. Amer. Meteor. Soc.,* **78,** 2539–2558.

Yang, D., B. E. Goodison, J. R. Metcalfe, V. S. Golubev, R. Bates, and T. Pangburn, 1998: Accuracy of NWS 8″ standard nonrecording precipitation gauge: Results and application of WMO intercomparison. *J. Atmos. Oceanic Technol.,* **15,** 54–68.

Yuter, S. E., and W. S. Parker, 2001: Rainfall measurement on ship revisited: The 1997 PACS TEPPS cruise. *J. Appl. Meteor.,* **40,** 1003–1018.